An Innovative Approach to the Design of Line-Start Permanent Magnet Synchronous Motors

Thanh Nguyen Vu
Laboratory of High-Performance Electric Machines (HiPEMs), Department of Electrical Engineering, School of Electrical and Electronic Engineering, Hanoi University of Science and Technology, Vietnam
thanh.nguyenvu@hust.edu.vn (corresponding author)

Dong Ngo Huy
Laboratory of High-Performance Electric Machines (HiPEMs), Department of Electrical Engineering, School of Electrical and Electronic Engineering, Hanoi University of Science and Technology, Vietnam
dong.nh222216m@sis.hust.edu.vn

Hoang Ha Quang
Laboratory of High-Performance Electric Machines (HiPEMs), Department of Electrical Engineering, School of Electrical and Electronic Engineering, Hanoi University of Science and Technology, Vietnam
hoang.hq200238@sis.hust.edu.vn

Vuong Dang Quoc
Laboratory of High-Performance Electric Machines (HiPEMs), Department of Electrical Engineering, School of Electrical and Electronic Engineering, Hanoi University of Science and Technology, Vietnam
vuong.dangquoc@hust.edu.vn

Chen Hao
School Electrical and Power Engineering, China University of Mining and Technology, Xuzhou, China
hchen@cumt.edu.cn

Received: 8 May 2025 | Revised: 24 June 2025 | Accepted: 3 July 2025

 DOI: https://doi.org/10.48084/etasr.11997

ABSTRACT

This paper describes an innovative analytical design approach for a Line-Start Permanent Magnet Synchronous Motor (LSPMSM) that can be used to swiftly verify the design parameters. The goal of the method is to create an analytical equation system based on the d-q coordinate system that considers both under-excitation and over-excitation scenarios. In this system, the essential design parameters of the LSPMSM motor are calculated and determined directly using the proposed equation system, namely the rated armature current (I_1), torque angle (δ), and phase difference (γ) between the induced electromotive force (E_{pm}) and the armature current. Three practical motors with rated outputs of 22 kW, 11 kW, and 3 kW were developed to investigate the accuracy of the proposed system. The results of the analytical method were compared with those of Finite Element Analysis (FEA), which revealed a high degree of suitability, with a relative error of less than ±5%. Furthermore, the proposed equation system's reliability was evaluated using two design parameters: the power factor and the effective value of the armature current, which were computed from the FEA-simulated current waveforms. The proposed equation system is a useful tool for the design verification and rapid optimization of LSPMSM motors because it significantly decreases the verification simulation time compared with FEA-based designs.

Keywords-torque angle; rated armature current; LSPMSM motor model; ultra premium efficiency; LSPMSM design

I. INTRODUCTION

The LSPMSM is a synchronous machine that combines the benefits of permanent magnet excitation with the self-starting capability of Induction Motors (IMs), made possible by its squirrel-cage rotor design. Because of its unique characteristics, the LSPMSM is regarded as a possible alternative to standard IMs in various industrial applications [1-

5]. Research has identified various advantages of LSPMSMs over asynchronous and electromagnetically excited synchronous motors. These benefits include lower rotor losses due to slip removal, increased energy efficiency, and higher power density. Under constant voltage load conditions, LSPMSMs can achieve IE5 efficiency [6, 7], resulting in a high-power factor, stable running speed, and significant energy savings. When combined with a power converter, LSPMSMs provide an outstanding thermal performance [2, 8]. Despite these advantages, researchers and engineers continue to face substantial technological challenges when designing LSPMSMs. Several studies have been conducted to address these issues, focusing on both theoretical analysis and experimental validation [4, 8-20]. A prominent research trend is converting existing IMs into LSPMSMs by utilizing the stator and frame structure of asynchronous machines while modifying the rotor to incorporate permanent magnets [4]. Several systematic design approaches have been proposed for LSPMSMs. These procedures typically include preliminary mathematical calculations, rotor structure optimization, and validation using FEA [11]. Advanced optimization approaches, such as genetic algorithms, have been also investigated to improve the rotor designs for optimal efficiency and power factors [13, 14]. Furthermore, changes in the rotor geometry, such as adding surface-mounted magnets or modifying the bridge structures, have been demonstrated to increase the synchronization and electromagnetic performance [12, 17-19].

Recearch has also focused on building direct design methods for LSPMSMs that combine insights from asynchronous motor design principles and Interior Permanent Magnet (IPM) motor optimization strategies [20]. Typically, the design process for prototype LSPMSMs involves three steps:

Step 1 entails applying analytical approaches to generate initial designs using analytical formulas and appropriate design algorithms [10, 21], with parameters iteratively changed to meet the desired objectives.

Step 2 validates the analytical results with FEM-based simulations to ensure their applicability, specifically by checking for electromagnetic alignment and acceptable thermal behavior [22, 23].

Step 3 includes creating prototype motors and experimentally testing them to ensure that the design meets the required performance standards [17, 24].

While there are many articles on the design of LSPMSM motors, most of these studies used analytical design methods and then checked their results utilizing FEM simulation models and experimental prototypes. This verification needs a considerable amount of simulation time, especially for 3D models, which require additional computational resources. To overcome the specific difficulty, this study proposes a novel solution to improve the efficiency and accuracy of the electromagnetic design process in step 1, focusing on the detailed determination and checking of the key parameters: the rated armature current (I_1), torque angle (δ), and phase difference (γ) between the electromotive force (E_{pm}) and I_1. These parameters are estimated using an analytical equation system based on the d-q coordinate framework, which considers both under-excited and over-excited operating conditions of the LSPMSM. The primary contributions of this study are the creation of a complete design procedure and an analytical equation system for the LSPMSM. To validate the proposed technique, the analytical results were compared with the FEM simulation results to guarantee consistency, correctness, and logical correlation. The proposed design method was applied and evaluated on three practical motors with rated outputs of 22 kW, 11 kW, and 3 kW to demonstrate the reliability and effectiveness of the proposed approach.

In the current work, a detailed approach to creating the analytical equation system for the three variables I_1, δ, and γ is presented to provide a quick check solution for these design parameters. The formulas utilized in the analytical design of the LSPMSM motor are provided to determine the parameters in the proposed equation system. The results obtained from solving the analytical equation system are analyzed for three motors rated at 22 kW, 11 kW, and 3 kW. The construction of these three motors is represented by a 2D-FEM model that is used to calculate and compare electromagnetic parameters, such as the steady-state armature current and power factor. In future work, this design solution will be applied to various magnet combinations on the rotor of an LSPMSM motor or will be combined with demagnetization related problems in LSPMSM motors during starting [25].

II. CONSTRUCTING A SYSTEM OF ANALYTICAL EQUATIONS USING THREE VARIABLEES

The LSPMSMs are classified as PMSMs. During operation, the machine can operate with either an under-excited or an over-excited motor. Hence, it is imperative to construct a set of equations that take into account both the under-excited and over-excited motor cases. The voltage phasor equations of the LSPMSM are defined as [26]:

$$\dot{U}_1 = \dot{E}_{pm} + \dot{I}_1 R_s + j\dot{I}_d X_d + j\dot{I}_q X_q \quad (1)$$

$$\dot{U}_1 = \dot{E}_{pm} + \dot{I}_d (R_s + jX_d) + \dot{I}_q (R_s + jX_q) \quad (2)$$

$$\dot{I}_1 = \dot{I}_d + \dot{I}_q \quad (3)$$

where U_1 is the phase voltage, E_{pm} is the electromotive force, I_1 is the rated armature current, I_d is the RMS d-axis current, I_q is the RMS q-axis current, R_s is the stator resistance, X_d is the synchronous reactance in the d-axis, *and* X_q is the synchronous reactance in the q-axis.

The phasor diagrams presented in Figures 1(a) and (b) can be constructed using (1), (2), and (3). According to the phasor diagram in Figure 1(a), the LSPMSM functions as a lagging load when $E_{pm}cos\delta < U_1$. The power grid provides reactive power to the motor because the current (I_1) lags in phase with the voltage (U_1). The motor is currently operating in a state of under-excitation.

However, the LSPMSM functions as a leading load when $E_{pm}cos\delta > U_1$ (Figure 1(b)), and the motor supplies reactive power to the grid because the current (I_1) is in phase with the voltage (U_1). The motor is currently operating in a state of over-excitation.

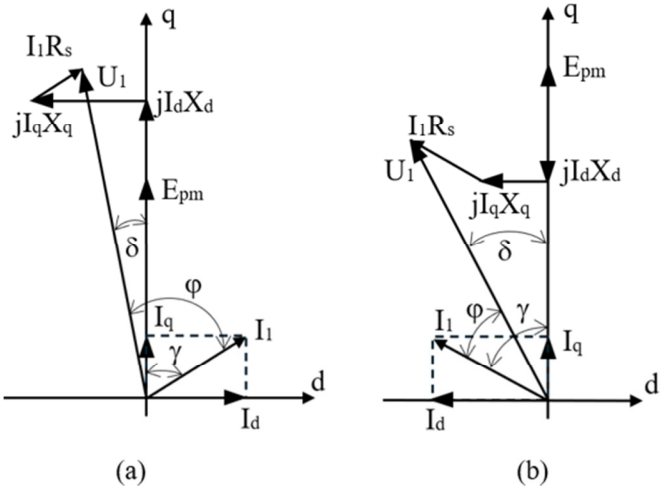

Fig. 1. Phasor diagrams of LSPMSMs: (a) a state of under-excitation, (b) a state of over-excitation.

By analyzing the phasor diagrams depicted in Figures 1(a) and (b), the equations listed in Table I were deduced.

TABLE I. EQUATIONS DERIVED FROM PHASE DIAGRAMS

Under-excited operation of LSPMSMs	
$U_1 sin\delta = I_q X_q - I_d R_s$	(4)
$U_1 cos\delta = E_{pm} + I_d X_d + I_q R_s$	(5)
$I_d = I_1 sin\gamma$	(6)
$I_q = I_1 cos\gamma$	(7)
$I_1 = \sqrt{(I_d)^2 + (I_q)^2} = \sqrt{(I_1 sin\gamma)^2 + (I_1 cos\gamma)^2}$	(8)
Over-excited operation of LSPMSMs	
$U_1 sin\delta = I_q X_q + I_d R_s$	(9)
$U_1 cos\delta = E_{pm} - I_d X_d + I_q R_s$	(10)
$I_d = -I_1 sin\gamma$	(11)
$I_q = I_1 cos\gamma$	(12)
$I_1 = \sqrt{(I_d)^2 + (I_q)^2} = \sqrt{(-I_1 sin\gamma)^2 + (I_1 cos\gamma)^2}$	(13)

Identical equations are obtained by applying transformations to the three variables I_1, δ, and γ from the equations in Table II, which pertain to the two scenarios of over-excitation and under-excitation:

$$I_1 sin\gamma = \frac{U_1(X_q cos\delta - R_s sin\delta) - E_{pm} X_q}{R_s^2 + X_d X_q} \quad (14)$$

$$I_1 cos\gamma = \frac{U_1(R_s cos\delta + X_d sin\delta) - E_{pm} R_s}{R_s^2 + X_d X_q} \quad (15)$$

The power losses are present in Δp_{fe}, Δp_m, Δp_{add}, and Δp_{cu} during the steady-state operation of the LSPMSM. The power balance equation in the LSPMSM is:

$$\sqrt{3} U_n I_1 cos(\gamma + \delta) = P_n + \Sigma\Delta P \quad (16)$$

The $\Sigma\Delta P$ and Δp_{fe} are given by:

$$\Sigma\Delta P = \Delta p_{fe} + \Delta p_m + \Delta p_{add} + \Delta p_{cu} \quad (17)$$

$$\Delta p_{fe} = \Delta p_{st} + \Delta p_{sy} \quad (18)$$

where Δp_{fe} represents the total core losses, Δp_{st} represents the iron losses in the stator tooth, Δp_{sy} represents the iron losses in the stator yoke, Δp_m represents the mechanical losses, Δp_{add} represents the additional losses, and Δp_{cu} represents the resistive losses in stator.

From the given transformations, it is evident that three variables, I_1, δ, and γ, need to satisfy (14), (15), and (16). Subsequently, a set of equations is proposed to determine the three variables:

$$\begin{cases} I_1 sin\gamma = \frac{U_1(X_q cos\delta - R_s sin\delta) - E_{pm} X_q}{R_s^2 + X_d X_q} \\ I_1 cos\gamma = \frac{U_1(R_s cos\delta + X_d sin\delta) - E_{pm} R_s}{R_s^2 + X_d X_q} \\ \sqrt{3} U_n I_1 cos(\gamma + \delta) = P_n + \Sigma\Delta P \end{cases} \quad (19)$$

However, the solutions must adhere to the following conditions:

$$I_1 = \sqrt{(I_1 sin\gamma)^2 + (I_1 cos\gamma)^2} \quad (20)$$

III. ANALYTICAL DESIGN OF LSPMSM

The comprehensive electromagnetic design of the LSPMSM motor and the computation of the parameters of the system of equations (19) were performed by following (21-37) [26, 27]. The design specifications of the three motors are given in Table II, where P_n is the rated power, η_n is the efficiency, U_n is the line voltage, and $cos\varphi_n$ is the power factor.

TABLE II. DESIGN SPECIFICATIONS OF THREE LSPMSMS WITH PHASE CONNECTIONS IN STAR

Parameters	22-kW motor	11-kW motor	3-kW motor
P_n (kW)	22	11	3
U_n (V)	380	380	380
η_n	0.95	0.93	0.93
$cos\varphi_n$	0.95	0.99	0.93
k_i	6.5	7	7.7
k_m	2.6	2.6	2.8

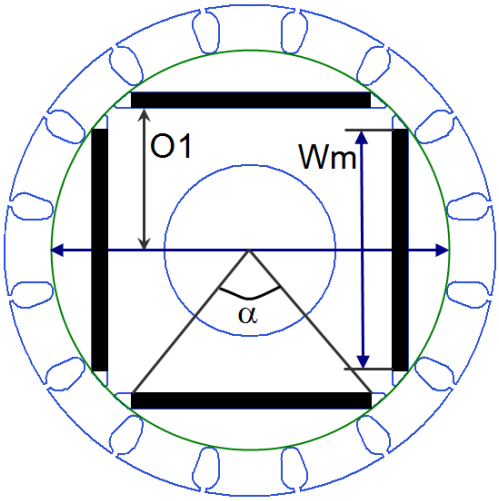

Fig. 2. Pole angle α of LSPMSM motor.

TABLE III. ANALYTICAL EQUATIONS [26, 27]

The rated armature current	
$I_1 = \frac{P_n}{\eta_n \sqrt{3} U_n cos\varphi_n}$	(21)
Electromotive force	
$E_{pm} = 4k_f k_w f \tau L_{pm} B_g W_1$ where k_f is the form factor, k_w is the stator winding factor, f is the frequency of power supply, τ is the pole pitch, L_{pm} is the magnet thickness, B_g is the airgap flux density, W_1 is the number of turns per phase.	(22)
The stator resistance	
$R_s = (1 + \alpha_T(t - t_0))(\rho_{cu})_{20} \frac{l_c W_1}{s_d a_1}$ where α_T is the temperature coefficient of resistance, $(\rho_{cu})_{20}$ is the copper resistivity at 20 °C, l_c is the coil length, s_d is the magnetic wire cross section, a_1 is the number of current paths in parallel.	(23)
The synchronous reactance in the d-axis	
$X_d = X_l + X_{ad}$ where X_l is the leakage reactance per phase of the armature windings, X_{ad} is the d-axis armature reaction reactance.	(24)
The d-axis armature reaction reactance	
$X_{ad} = 4m\mu_0 f \frac{(W_1 k_w)^2 \tau L_{pm} k_{fd}}{\pi p g'}$ where m is the number of phases, μ_0 is the magnetic permeability of free space, k_{fd} is the d-axis form factor of the armature reaction, g' is the equivalent air gap.	(25)
The d-axis form factor of the armature reaction	
$k_{fd} = \frac{1}{\pi}\left(\left(\frac{k_c g}{g'}\right)(2\alpha - sin(2\alpha)) + \pi + sin(2\alpha) - 2\alpha\right)$ where g is the air gap, k_c is the Caster factor, α is the pole angle (as shown in Figure 2) $\alpha = 2\frac{180}{\pi} artan\left(\frac{Wm}{2*01}\right)$.	(26)
The synchronous reactance in the q-axis	
$X_q = X_l + X_{aq}$ where X_{aq} is the d-axis armature reaction reactance.	(27)
The q-axis armature reaction reactance	
$X_{aq} = 4m\mu_0 f \frac{(W_1 k_w)^2 \tau L_{pm} k_{fq}}{\pi p g'}$ where k_{fq} is the q-axis form factor of the armature reaction.	(28)
The q-axis form factor of the armature reaction	
$k_{fq} = \frac{1}{\pi}\left(\left(\frac{k_c g}{g'}\right)(2\alpha + sin(2\alpha)) + \pi - sin(2\alpha) - 2\alpha\right)$	(29)
The torque angle characteristics	
$T_d = \frac{3p}{2\omega_s}.\frac{E_{pm}.U_1}{X_d} sin\delta + \frac{3p}{2\omega_s}.\frac{U_1^2}{2}\left(\frac{1}{X_q} - \frac{1}{X_d}\right) sin2\delta$ where ω_s is the synchronous angular velocity.	(30)
The synchronous torque	
$T_{syn} = \frac{3p}{2\omega_s}.\frac{E_{pm}.U_1}{X_d} sin\delta$	(31)
The reluctance torque	
$T_{rel} = \frac{3p}{2\omega_s}.\frac{U_1^2}{2}\left(\frac{1}{X_q} - \frac{1}{X_d}\right) sin2\delta$	(32)
The iron losses in the stator tooth	
$\Delta p_{st} = k_t p_{10} \left(\frac{f}{50}\right)^{1.3} B_{ts}^{1.7} G_{t1}$ where k_t accounts for core loss augmentation due to mechanical machining, p_{10} is the specific losses, B_{ts} is the stator tooth flux density, G_{t1} is the stator tooth weight.	(33)
The iron losses in the stator yoke	
$\Delta p_{sy} = k_y p_{10} \left(\frac{f_1}{50}\right)^{1.3} B_{sy}^{1.7} G_{y1}$ where k is the influence of mechanical machining, B_{sy} is the stator yoke flux density, G_{y1} is the stator yoke weight.	(34)
The mechanical losses	
$\Delta P_m = \left(\frac{n_n}{1000}\right)^2 \left(\frac{D_o}{100}\right)^4$ where n_n is the rotor speed and D_o is the stator outer diameter.	(35)
The additional losses	
$\Delta P_{add} = 0{,}01.P_n$	(36)
The resistive losses in stator.	
$\Delta P_{cu} = 3R_s I_1^2$	(37)

Based on (21-37), the practical parameters for the three motors with ratings of 22, 11, and 3 kW were computed. The results for the three proposed motors are shown in Table IV. These values serve as the input parameters for the system of equations (19) in the second section of this paper.

TABLE IV. THE PRACTICAL PARAMETERS OF THREE LSPMSM MOTORS: 22 KW, 11 KW, AND 3 KW

Parameters	22-kW motor	11-kW motor	3-kW motor	Unit
P_n	22	11	3	kW
U_l	380	380	380	V
T_d	140.06	70.03	19.1	Nm
X_d	4.241	4.702	4.459	Ω
X_q	7.597	8.288	11.796	Ω
E_{pm}	211.93	199.18	209.316	V
R_s	0.19	0.5	1.58	Ω
Δp_{fe}	314.99	190.45	112.64	W
Δp_m	264	132	14.02	W
Δp_{add}	220	110	30	W
Δp_{cu}	$0.57I_1^2$	$1.5I_1^2$	$4.74I_1^2$	W

IV. RESULTS AND DISCUSSION

A. Analytical Results

By substituting the parameters of Table IV into the system of equations (19), a system of analytical equations with three variables and conditional inequality is derived. The system of analytical equations with three variables is shown in Table V.

TABLE V. THE PROPOSED SYSTEM OF EQUATIONS INVOLVING THREE MOTORS WITH CAPACITIES OF 22 KW, 11 KW, AND 3 KW

For a motor of 22 kW	
$\begin{cases} 658.19I_1 cos(\gamma + \delta) = 22841.92 + 0.57I_1^2 \\ 32.25I_1 sin(\gamma) = 1671.34cos(\delta) - 41.8sin(\delta) - 1610.03 \\ 32.25I_1 cos(\gamma) = 41.8cos(\delta) + 933.02sin(\delta) - 40.27 \end{cases}$	(38)
For a motor of 11 kW	
$\begin{cases} 658.19I_1 cos(\gamma + \delta) = 11432.45 + 1.5I_1^2 \\ 39.22I_1 sin(\gamma) = 1823.36cos(\delta) - 110sin(\delta) - 1650.80 \\ 39.22I_1 cos(\gamma) = 110cos(\delta) + 1034.44sin(\delta) - 99.59 \end{cases}$	(39)
For a motor of 3 kW	
$\begin{cases} 658.19I_1 cos(\gamma + \delta) = 3178.63 + 4.74I_1^2 \\ 634.53I_1 sin(\gamma) = 4463.8cos(\delta) - 347.6sin(\delta) - 4247.02 \\ 634.53I_1 cos(\gamma) = 347.6cos(\delta) + 6853sin(\delta) - 330.72 \end{cases}$	(40)
Conditional equality is used for (38), (39), and (40).	
$I_1 = \sqrt{(I_1 \sin\gamma)^2 + (I_1 \cos\gamma)^2}$	(41)

By solving (38), (39), and (40) and meeting the condition in (41), the results shown in Table VI are obtained and compared to the FEA results in Table VII.

Also, by solving (30), (31), and (32), the torque angle characteristics of three LSPMSM motors with power ratings of 22 kW, 11 kW, and 3 kW are displayed in Figures 3-5, respectively. It is evident that the rated torque value (T_d) and torque angle d match well with the torque angle d values listed in Table VI.

TABLE VI. RESULTS OF THE PROPOSED SYSTEMS OF EQUATIONS

For motor of 22kW	**For motor of 11kW**
$\begin{cases} I_1 = 37.22862\ (A) \\ \delta = 1.09844\ (rad) \\ \gamma = -0.83088\ (rad) \\ \varphi = \delta + \gamma = 0.26756\ (rad) \\ Cos\varphi = 0.964 \end{cases}$	$\begin{cases} I_1 = 18.67\ (A) \\ \delta = 0.70319\ (rad) \\ \gamma = -0.46912\ (rad) \\ \varphi = \delta + \gamma = 0.23406\ (rad) \\ Cos\varphi = 0.973 \end{cases}$
For motor of 3kW	
$\begin{cases} I_1 = 5.38\ (A) \\ \delta = 0.51912\ (rad) \\ \gamma = -0.15993\ (rad) \\ \varphi = \delta + \gamma = 0.35919\ (rad) \\ Cos\varphi = 0.936 \end{cases}$	

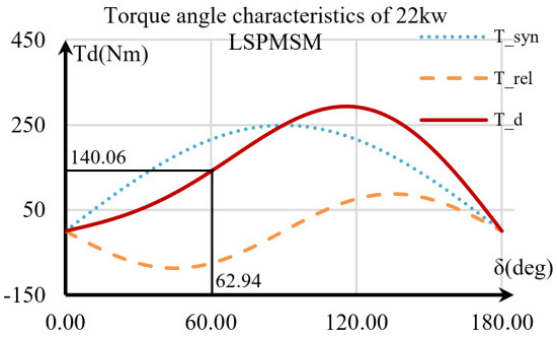

Fig. 3. Torque–angle characteristics of the 22 kW LSPMSM.

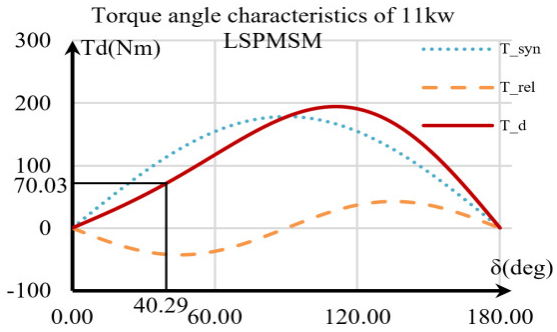

Fig. 4. Torque–angle characteristics of the 11 kW LSPMSM.

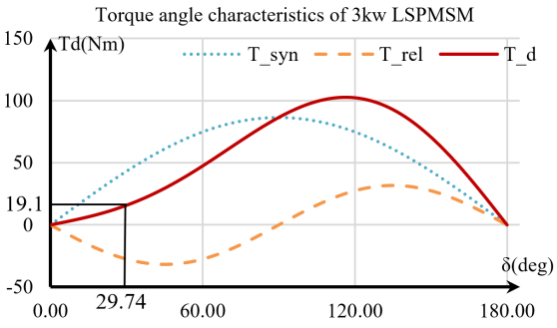

Fig. 5. Torque–angle characteristics of the 3 kW LSPMSM.

B. *Numerical Results*

To validate the accuracy of the analytical models presented above, three LSPMSMs with rated powers of 22 kW, 11 kW, and 3 kW were simulated using the Altar Flux 2D software. Figures 6-8 illustrate the flux density distributions for the three LSPMSM motors. The magnet bridge area typically displays the highest flux density due to its relatively narrow cross-section, which leads to a significant concentration of flux density. The 22-kW motor exhibits a maximum flux density of 2.092 T, while the 11-kW motor has a maximum of 2.145 T. In contrast, the 3-kW motor demonstrates a maximum flux density of 2.79 T.

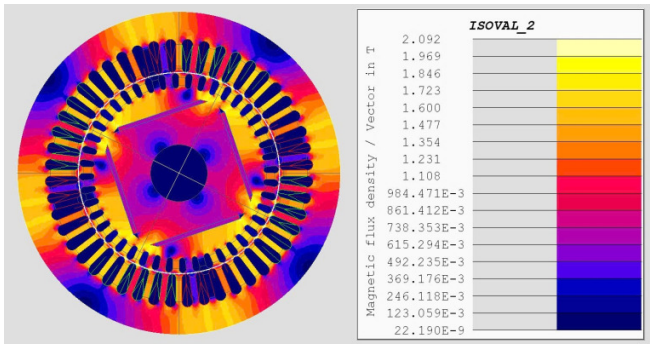

Fig. 6. Distribution of magnetic flux density on the 22 kW motor.

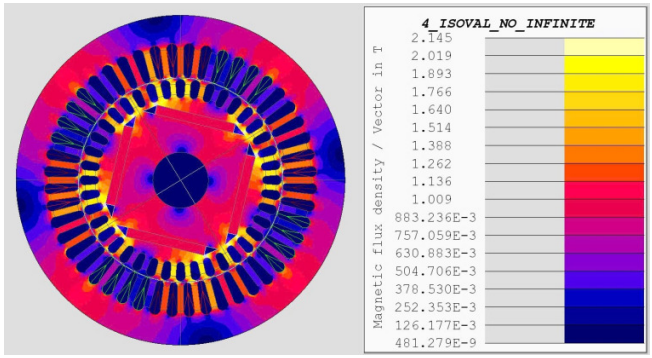

Fig. 7. Distribution of magnetic flux density on the 11 kW motor.

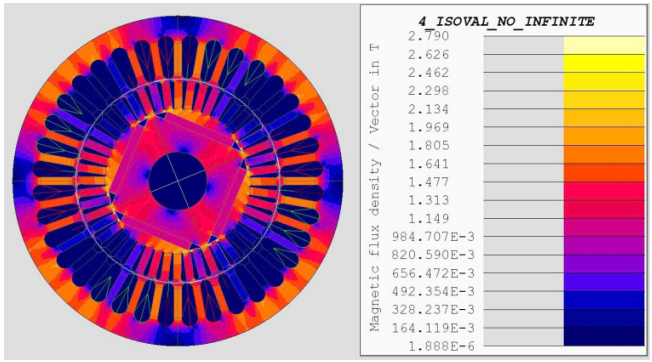

Fig. 8. Distribution of magnetic flux density on the 3 kW motor.

Figures 9-11 show that in a steady state, the peak values of the rated armature current waveforms are 52.52 A, 27.29 A, and 7.27 A for motors rated at 22 kW, 11 kW, and 3 kW,

respectively. The RMS current values for the motors are 37.23 A for the 22-kW motor, 19.29 A for the 11-kW motor, and 5.14 A for the 3-kW motor. Table VII compares the values of the rated armature current determined using (21), calculated from the proposed equation system of (19), and using the FEA simulation model. All values presented in Table VII are within an acceptable error range of ±5%.

TABLE VII. COMPARISON OF THE RATED ARMATURE CURRENT

Motor	I_1 determined by (21)	I_1 solved by (19)	I_1 determined by the FEA simulation model
22-kW	37.04 (A)	37.23 (A)	37.14 (A)
11-kW	18.15 (A)	18.67 (A)	19.3 (A)
3-kW	5.27 (A)	5.38 (A)	5,14 (A)

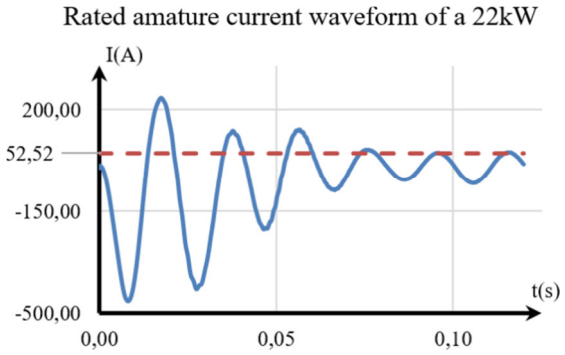

Fig. 9. Rated armature current waveform of a 22 kW.

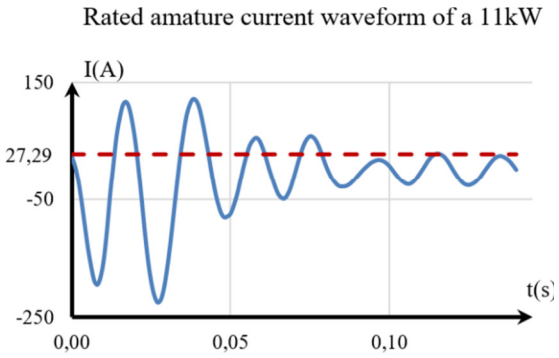

Fig. 10. Rated armature current waveform of a 3 kW.

In a steady state, the phase difference φ between the phase voltage and phase current is calculated directly from the waveforms of the three motors: 22 kW, 11 kW, and 3 kW. The simulation results in Figures 12-14 reveal that all three motors operate in a state of under-excitation, which means that the phase current lags the phase voltage. The lag time for the 22-kW motor was 0.00107 s, which corresponds to a 19.260 angle difference. The lag time for the 11-kW motor was 0.0000573 s, which corresponds to a 1.030 angle difference. The lag time for the 3-kW motor was 0.001072 s, which corresponds to a 19.260 angle difference. Table VIII displays the results of the power factors, which are similar to the results obtained by solving (19). The errors for each motor, 22, 11, and 3 kW, were 2.1%, -2.67%, and -0.85%, respectively. All errors were within the allowed range of ±5%.

TABLE VIII. PHASE SHIFT AND DIFFERENCE OF THREE MOTORS

Motor	$\varphi = \frac{\Delta t}{T}.360^0$	Cosφ is computed from the FEA simulation model	Cosφ is solved by the system of equations (19)
22-kW	19.26^0	0.944	0.964
11-kW	1.03^0	0.999	0.973
3-kW	19.26^0	0.944	0.936

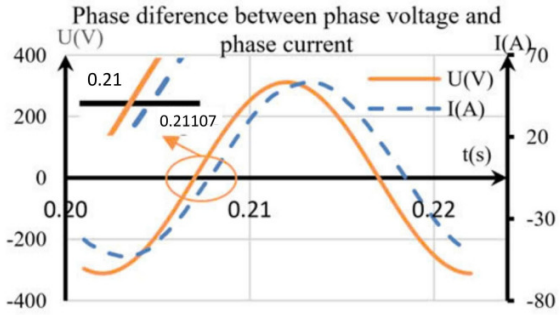

Fig. 11. Phase difference between phase voltage and phase current of the 22-kW motor.

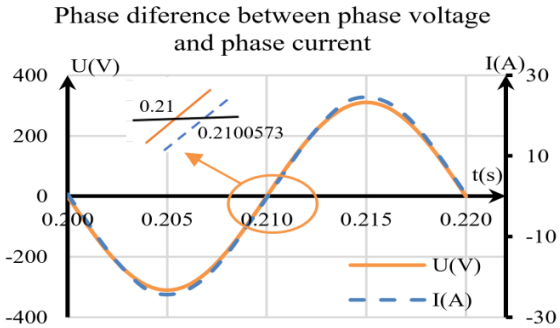

Fig. 12. Phase difference between phase voltage and phase current of the 11-kW motor.

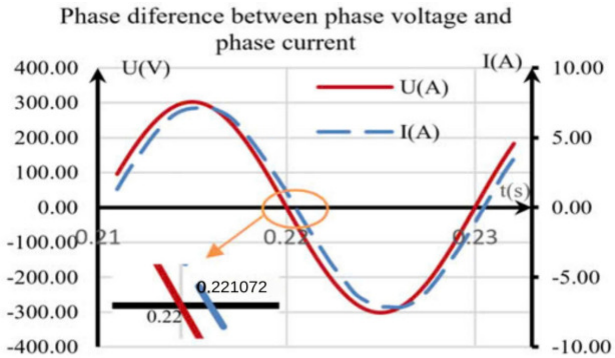

Fig. 13. Phase difference between phase voltage and phase current of the 3-kW motor.

V. CONCLUSIONS

This study introduces a novel and efficient approach to the electromagnetic design of Line-Start Permanent Magnet Synchronous Motors (LSPMSMs) by developing an analytical equation system based on the d–q coordinate framework. The proposed system of equations considers both a state of under-excitation and over-excitation and enables the direct calculation

of key design parameters, including the rated armature current (I_1), torque angle (δ), and phase difference (γ) between the electromotive force (E_{pm}) and I_1. This method offers a rapid yet accurate means of evaluating LSPMSM designs during early stages. The proposed design methodology was applied to three motors with rated powers of 22 kW, 11 kW, and 3 kW. The analytical results obtained from solving the equation system were validated through Finite Element Analysis (FEA), showing strong agreement with relative errors maintained within ±5%. Furthermore, the current waveform analysis and phase difference evaluations confirm that all tested motors operated in an under-excited state, and the computed power factors closely. In comparison with conventional FEM-based design procedures, which require significant computation time (typically 3–4 h), the proposed analytical method produces results within a few tenths of seconds, highlighting its practical advantages for rapid prototyping and design iteration. This efficiency can substantially reduce the development time and resource consumption, particularly in design optimization processes.

Future work will explore the application of this analytical design method to LSPMSMs employing different permanent magnet configurations, aiming to further enhance the design flexibility and motor performance

ACKNOWLEDGEMENTS

The authors would like to thank The Laboratory of High-Performance Electric Machines (HiPEMs), Department of Electrical Engineering, Hanoi University of Science and Technology, Vietnam for their facilities and constructive criticism of the manuscript.

REFERENCES

[1] K. J. Binns, W. R. Barnard, and M. A. Jabbar, "Hybrid permanent-magnet synchronous motors," *Proceedings of the Institution of Electrical Engineers*, vol. 125, no. 3, pp. 203–208, Mar. 1978, https://doi.org/10.1049/piee.1978.0053.

[2] A. T. de Almeida, F. J. T. E. Ferreira, and G. Baoming, "Beyond Induction Motors—Technology Trends to Move Up Efficiency," *IEEE Transactions on Industry Applications*, vol. 50, no. 3, pp. 2103–2114, May 2014, https://doi.org/10.1109/TIA.2013.2288425.

[3] M. F. Palangar, W. L. Soong, and A. Mahmoudi, "Outer and Inner Rotor Line-Start Permanent-Magnet Synchronous Motors: An Electromagnetic and Thermal Comparison Study," in *2021 IEEE Energy Conversion Congress and Exposition (ECCE)*, Vancouver, BC, Canada, Oct. 2021, pp. 4226–4233, https://doi.org/10.1109/ECCE47101.2021.9595574.

[4] W. Fei, P. C. K. Luk, J. Ma, J. X. Shen, and G. Yang, "A High-Performance Line-Start Permanent Magnet Synchronous Motor Amended From a Small Industrial Three-Phase Induction Motor," *IEEE Transactions on Magnetics*, vol. 45, no. 10, pp. 4724–4727, Oct. 2009, https://doi.org/10.1109/TMAG.2009.2022179.

[5] P. Sethupathi and N. Senthilnathan, "Comparative analysis of line-start permanent magnet synchronous motor and squirrel cage induction motor under customary power quality indices," *Electrical Engineering*, vol. 102, no. 3, pp. 1339–1349, Sep. 2020, https://doi.org/10.1007/s00202-020-00955-2.

[6] B.-A. Kerslake, A. Mahmoudi, and S. Kahourzade, "Line-Start Permanent-Magnet Synchronous Motor versus Induction Motor: Technical, Environmental and Economical Considerations," in *2021 IEEE 12th Energy Conversion Congress & Exposition - Asia (ECCE-Asia)*, Singapore, Singapore, May 2021, pp. 857–864, https://doi.org/10.1109/ECCE-Asia49820.2021.9479424.

[7] M. Gwozdziewicz and K. Jankowska, "Analysis of a new concept of Line Start Permanent Magnet Synchronous Motor," *Przegląd Elektrotechniczny*, vol. 98, no. 8, pp. 168–173, Aug. 2022, https://doi.org/10.15199/48.2022.08.31.

[8] M. Gwozdziewicz and M. Ciurys, "Line start permanent magnet synchronous motorrotor designing methodology," *Przegląd Elektrotechniczny*, vol. 99, no. 12, 2023, Art. no. 146739, https://doi.org/10.15199/48.2023.12.40.

[9] M. J. Melfi, S. D. Umans, and J. E. Atem, "Viability of Highly Efficient Multi-Horsepower Line-Start Permanent-Magnet Motors," *IEEE Transactions on Industry Applications*, vol. 51, no. 1, pp. 120–128, Jan. 2015, https://doi.org/10.1109/TIA.2014.2347239.

[10] J. Li, J. Song, and Y. Cho, "High performance line start permanent magnet synchronous motor for pumping system," in *2010 IEEE International Symposium on Industrial Electronics*, Bari, Jul. 2010, pp. 1308–1313, https://doi.org/10.1109/ISIE.2010.5637082.

[11] S. S. Patil, R. T. Ugale, A. Kumar, and S. S. Revalkar, "Design of Line Start Linear Permanent Magnet Synchronous Motor for Electromagnetic Catapult," in *IECON 2020 The 46th Annual Conference of the IEEE Industrial Electronics Society*, Singapore, Oct. 2020, pp. 920–925, https://doi.org/10.1109/IECON43393.2020.9255117.

[12] A. Waheed, B. Kim, and Y.-H. Cho, "Optimal Design of Line-Start Permanent Magnet Synchronous Motor Based on Magnetic Equivalent Parameters," *Journal of Electrical Engineering & Technology*, vol. 15, no. 5, pp. 2111–2119, Sep. 2020, https://doi.org/10.1007/s42835-020-00464-z.

[13] B. Zöhra, M. Akar, and M. Eker, "Design of A Novel Line Start Synchronous Motor Rotor," *Electronics*, vol. 8, no. 1, Jan. 2019, Art. no. 25, https://doi.org/10.3390/electronics8010025.

[14] M. F. Palangar, A. Mahmoudi, S. Kahourzade, and W. L. Soong, "Optimum Design of Line-Start Permanent-Magnet Synchronous Motor Using Mathematical Method," in *2020 IEEE Energy Conversion Congress and Exposition (ECCE)*, Detroit, MI, USA, Oct. 2020, pp. 2064–2071, https://doi.org/10.1109/ECCE44975.2020.9236205.

[15] H.-J. Park, H.-B. Hong, and K.-D. Lee, "A Study on a Design Considering the Transient State of a Line-Start Permanent Magnet Synchronous Motor Satisfying the Requirements of the IE4 Efficiency Class," *Energies*, vol. 15, no. 24, Jan. 2022, Art. no. 9644, https://doi.org/10.3390/en15249644.

[16] S. Kahourzade, A. Mahmoudi, W. P. Hew, and M. N. Uddin, "Design and performance improvement of a line-start PMSM," in *2013 IEEE Energy Conversion Congress and Exposition*, Sep. 2013, pp. 5042–5047, https://doi.org/10.1109/ECCE.2013.6647381.

[17] H. Kim, J. Lee, J. Kang, and J. Kim, "Rotor Design for Improving the Maximum Inertia and Power Factor in Line-Start Synchronous Reluctance Motor," in *2022 IEEE 20th Biennial Conference on Electromagnetic Field Computation (CEFC)*, Oct. 2022, pp. 1–2, https://doi.org/10.1109/CEFC55061.2022.9940898.

[18] M. Si, X. Yu, and B. Wu, "Design and Analysis of a Novel Line-Start Permanent-Magnet Synchronous Motor," in *2019 22nd International Conference on Electrical Machines and Systems (ICEMS)*, Harbin, China, Aug. 2019, pp. 1–4, https://doi.org/10.1109/ICEMS.2019.8922496.

[19] B. Yan, Y. Yang, and X. Wang, "Design of a Large Capacity Line-Start Permanent Magnet Synchronous Motor Equipped With Hybrid Salient Rotor," *IEEE Transactions on Industrial Electronics*, vol. 68, no. 8, pp. 6662–6671, Aug. 2021, https://doi.org/10.1109/TIE.2020.3008360.

[20] T. Ding, N. Takorabet, F.-M. Sargos, and X. Wang, "Design and Analysis of Different Line-Start PM Synchronous Motors for Oil-Pump Applications," *IEEE Transactions on Magnetics*, vol. 45, no. 3, pp. 1816–1819, Mar. 2009, https://doi.org/10.1109/TMAG.2009.2012772.

[21] J. M. Lee, "A Comparison of Salient and Nonsalient Pole Line-Start Permanent Magnet Synchronous Machines," 1997, https://doi.org/10.13140/RG.2.2.30720.12803.

[22] İ. Tarımer, "Investigation of the Effects of Rotor Pole Geometry and Permanent," *Elektronika ir Elektrotechnika*, vol. 90, no. 2, pp. 67–72, Feb. 2009.

[23] T. Marcic, "A short review of energy-efficient line-start motor design," *Przegląd Elektrotechniczny (Electrical Review)*, vol. 87, no. 3, pp. 119–122, 2011.

[24] B. Zöhra and M. Akar, "Performance verification of novel rotor line start PMSM," *Journal of Mechatronics and Artificial Intelligence in Engineering*, vol. 2, no. 2, pp. 86–95, Dec. 2021, https://doi.org/10.21595/jmai.2021.22219.

[25] T. L. Anh, T. T. Bien, C. N. Xuan, T. D. Anh, and Y. D. Nhu, "Analysis of Permanent Magnet Demagnetization during the Starting Process of a Line-start Permanent Magnet Synchronous Motor," *Engineering, Technology & Applied Science Research*, vol. 14, no. 6, pp. 17900–17905, Dec. 2024, https://doi.org/10.48084/etasr.8576.

[26] J. F. Gieras, *Permanent Magnet Motor Technology: Design and Applications*. CRC Press, 2009.

[27] I. Boldea and S. A. Nasar, *The Induction Machines Design Handbook*, 2nd ed. Boca Raton, FL: CRC Press, 2010.

AUTHORS PROFILE

Thanh Nguyen Vu is an Assistant Professor in the Department of Electrical Engineering, School of Electronic and Electric Engineering, Hanoi University of Science and Technology, Vietnam. He received his MSc (Electrical Engineering) from Hanoi University of Science and Technology, Vietnam in 2002 and Ph.D (Electrical Engineering) from the same University in 2016. Both his MSc and Ph.D dissertations focused on rotating machine efficiency and optimizing motor design. He has teaching experience of more than 20 years in the areas of electrical machines. Dr. Thanh Nguyen Vu is an electrical engineer, researcher, and assistant professor specializing in high-efficiency motors and sustainable energy solutions. Currently, he is the Head of the Department of Electrical Engineering, School of Electronic and Electric Engineering, Hanoi University of Science and Technology, Vietnam. His research encompasses the modeling of electrical machines, optimization and numerical methods. He can be contacted via email: thanh.nguyenvu@hust.edu.vn.

Dong Ngo Huy received the master degree in electrical engineering in 2024 from the Department of Electrical Engineering, School of Electronic and Electric Engineering, Hanoi University of Science and Technology, Vietnam. He is currently a PhD student at the same institution. He is highly interested in performing finite element analysis for the optimal design of permanent magnet synchronous motors. He can be contacted at email: dong.nh222216m@sis.hust.edu.vn

Hoang Ha Quang received the bachelor degree in electrical engineering in 2024 from the Department of Electrical Engineering, School of Electronic and Electric Engineering, Hanoi University of Science and Technology, Vietnam. He is currently working as a master's student at the same institution. He is highly interested in simulating permanent magnet synchronous motors using the finite element method. He can be contacted at email: hoang.hq200238@sis.hust.edu.vn

Vuong Dang Quoc received his PhD in 2013 from the Faculty of Applied Sciences at the University of Liège, Belgium. After that, he returned to the Hanoi University of Science and Technology in September 2013, where he is currently working as deputy director of the Training Center of Electrical Engineering, School of Electrical Engineering, Hanoi, University of Science and Technology. He became an associate professor in 2020. Assoc. Prof. Dang Quoc Vuong's research domain encompasses modeling of electromagnetic systems, electrical machines, optimization method, numerical methods and subproblem methods. He can be contacted via email: vuong.dangquoc@hust.edu.vn.

Chen Hao received the B.S. and Ph.D. degrees in Electrical Engineering from the Department of Automatic Control, Nanjing University of Aeronautics and Astronautics, Nanjing, China, in 1991 and 1996, respectively. In 1998, he became an Associate Professor with the School of Information and Electrical Engineering, China University of Mining and Technology, Xuzhou, China, where he has been a professor since 2001. From 2002 to 2003, he was a Visiting Professor at Kyungsung University, Busan, Korea. Since 2008, he has also been an Adjunct Professor at the University of Western Australia, Perth, Australia. He is the author of one book and has also authored more than 200 papers. He is the holder of 15 US Patents, 23 Australian Patents, 1 Danish Patent, 7 Canadian Patents, 3 South African Patents, 10 Russian Patents, 66 Chinese Invention Patents and 6 Chinese Utility Model Patents. His current research interests include motor control, linear launcher, electric vehicles, electric traction, servo drives, and wind power generator control. Prof. Chen was the recipient of both the Prize of Science and Technology of Chinese Youth and the Prize of the Fok Ying Tong Education Foundation for Youth Teachers in both 2004).